



**HAL**  
open science

## Performance of MAX-DOAS measurements of aerosols at Tsukuba, Japan: a comparison with lidar and sky radiometer measurements

H. Irie, Y. Kanaya, H. Akimoto, H. Iwabuchi, A. Shimizu, K. Aoki

► **To cite this version:**

H. Irie, Y. Kanaya, H. Akimoto, H. Iwabuchi, A. Shimizu, et al.. Performance of MAX-DOAS measurements of aerosols at Tsukuba, Japan: a comparison with lidar and sky radiometer measurements. *Atmospheric Chemistry and Physics Discussions*, 2007, 7 (4), pp.9769-9793. hal-00302951

**HAL Id: hal-00302951**

**<https://hal.science/hal-00302951>**

Submitted on 18 Jun 2008

**HAL** is a multi-disciplinary open access archive for the deposit and dissemination of scientific research documents, whether they are published or not. The documents may come from teaching and research institutions in France or abroad, or from public or private research centers.

L'archive ouverte pluridisciplinaire **HAL**, est destinée au dépôt et à la diffusion de documents scientifiques de niveau recherche, publiés ou non, émanant des établissements d'enseignement et de recherche français ou étrangers, des laboratoires publics ou privés.

# Performance of MAX-DOAS measurements of aerosols at Tsukuba, Japan: a comparison with lidar and sky radiometer measurements

H. Irie<sup>1</sup>, Y. Kanaya<sup>1</sup>, H. Akimoto<sup>1</sup>, H. Iwabuchi<sup>1</sup>, A. Shimizu<sup>2</sup>, and K. Aoki<sup>3</sup>

<sup>1</sup>Frontier Research Center for Global Change, Japan Agency for Marine-Earth Science and Technology, 3173-25 Showa-machi, Kanazawa-ku, Yokohama, Kanagawa 236-0001, Japan

<sup>2</sup>National Institute for Environmental Studies, 16-2, Onogawa, Tsukuba, Ibaraki 305-8506, Japan

<sup>3</sup>Department of Earth Science, Faculty of Sciences, University of Toyama, 3190 Gofuku, Toyama 930-8555, Japan

Received: 30 May 2007 – Accepted: 28 June 2007 – Published: 5 July 2007

Correspondence to: H. Irie (irie@jamstec.go.jp)

Performance of  
MAX-DOAS  
measurements of  
aerosols in Japan

H. Irie et al.

Title Page

Abstract

Introduction

Conclusions

References

Tables

Figures

⏪

⏩

◀

▶

Back

Close

Full Screen / Esc

Printer-friendly Version

Interactive Discussion

## Abstract

Ground-based Multi-Axis Differential Optical Absorption Spectroscopy (MAX-DOAS) measurements were performed at Tsukuba, Japan (36.1° N, 140.1° E), in November–December 2006. The measured spectra of scattered sunlight are analyzed by DOAS and optimal estimation methods to retrieve the aerosol optical depth ( $\tau$ ) and the vertical profile of the aerosol extinction coefficient ( $\sigma$ ) at 476 nm in the lower troposphere. We characterize these retrieved quantities through comparisons with coincident lidar and sky radiometer measurements. The retrieved  $\sigma$  values for layers of 0–1 and 1–2 km agree with lidar data to within 30% and 60%, respectively, for most cases, including partly cloudy conditions. Results similar to  $\sigma$  at 0–1 km are obtained for the retrieved  $\tau$  values, demonstrating that MAX-DOAS provides the new, unique aerosol dataset in the lower troposphere.

## 1 Introduction

Atmospheric aerosols reflect and absorb solar radiation and modify cloud properties, altering the Earth's radiation balance and hence climate. A major uncertainty in the prediction of the future climate changes arises from the difficulty of modeling the effects of atmospheric aerosols. Because aerosols impact both regional and global energy budgets, owing to their highly non-uniform spatial and temporal distributions in the troposphere, a multiple-measurement approach is highly desirable to assess their impacts on the Earth's system (Kaufman et al., 2002).

Recently, the ground-based Multi-Axis Differential Optical Absorption Spectroscopy (MAX-DOAS) technique has been proposed as a new technique to measure aerosol optical properties, including the aerosol optical depth ( $\tau$ ) and the vertical profile of the aerosol extinction coefficient ( $\sigma$ ) in the visible wavelength region (Wagner et al., 2004; Frieß et al., 2006). The MAX-DOAS technique basically utilizes the differential absorption structures of the oxygen dimer ( $O_2-O_2$  or  $O_4$ ) for deriving aerosol informa-

### Performance of MAX-DOAS measurements of aerosols in Japan

H. Irie et al.

Title Page

Abstract

Introduction

Conclusions

References

Tables

Figures

⏪

⏩

◀

▶

Back

Close

Full Screen / Esc

Printer-friendly Version

Interactive Discussion

tion. Because no absolute radiometric calibrations are generally needed, MAX-DOAS is suitable for conducting long-term measurements in a consistent manner. In addition, MAX-DOAS measurements can yield significant information about several important trace gases, such as nitrogen dioxide (NO<sub>2</sub>), formaldehyde, and glyoxal (e.g. Hönninger et al., 2004; Wittrock et al., 2004; Heckel et al., 2005; Hendrick et al., 2006; Leigh et al., 2006; Sinreich et al., 2007), and thus have a variety of potential applications for understanding the Earth's system. Necessary input parameters for trace gas retrievals are given by the derived aerosol properties. However, the quantitative assessment of the MAX-DOAS aerosol measurements, particularly based on the comparison with other measurements, has been very limited.

Here we present ground-based MAX-DOAS measurements performed at Tsukuba, Japan (36.1° N, 140.1° E, 29 m a.s.l.), from 1 November to 21 December, 2006. Our retrieval algorithm for determining  $\tau$  and the vertical profile of  $\sigma$  at a wavelength ( $\lambda$ ) of 476 nm is presented. The wavelength of 476 nm corresponds to the O<sub>4</sub>-cross-section-weighted mean wavelength over the fitting window chosen for the spectral fitting (460–490 nm). We next show comparisons with lidar and sky radiometer measurements conducted at the same site. Although the geometry and the integration time for completing a set of the MAX-DOAS measurements are different from those of the lidar and sky radiometer, we attempt to estimate the overall uncertainty of the retrieved  $\sigma$  values for layers of 0–1 and 1–2 km, to which the sensitivity of MAX-DOAS measurements has been simulated to be much higher than at other altitudes (Frieß et al., 2006). Limitations in the retrieval of  $\tau$  are discussed based on the comparisons with sky radiometer and lidar data.

---

**Performance of  
MAX-DOAS  
measurements of  
aerosols in Japan**H. Irie et al.

---

[Title Page](#)[Abstract](#)[Introduction](#)[Conclusions](#)[References](#)[Tables](#)[Figures](#)[⏪](#)[⏩](#)[◀](#)[▶](#)[Back](#)[Close](#)[Full Screen / Esc](#)[Printer-friendly Version](#)[Interactive Discussion](#)

## 2 Measurement and retrieval algorithm

### 2.1 MAX-DOAS

Our MAX-DOAS instrument consists of two main parts: a telescope unit placed outdoors and a miniaturized UV/visible spectrometer (B&W TEK Inc., BTC111) indoors. These are connected via a 3-m fiber-optic bundle cable consisting of seven cores, each of which having a diameter of 100  $\mu\text{m}$ . The telescope unit has two viewing quartz windows, one for the zenith and one for off-axis directions. The line of sight for off-axis geometries was directed northwest. A movable mirror on a rotary actuator was installed inside the telescope unit, allowing a sequential measurement of scattered sunlight at six different elevation angles (ELs) of 3°, 5°, 10°, 20°, 30°, and 90° every 30 min. A plano-convex lens (focal length=40 mm and diameter=25 mm) focuses the received sunlight onto the fiber. The field of view (FOV) was estimated to be  $<1^\circ$ . The spectrometer employs a 10- $\mu\text{m}$  width slit, a Crossed Czerny-Turner optical layout, a plane-ruled grating with a groove frequency of 1800 lines  $\text{mm}^{-1}$  at a blaze wavelength of 250 nm, a thermoelectrically cooled linear charge-coupled device (CCD) array (ILX511, Sony) with 2048 elements covering a wavelength region of 283–566 nm, and a built-in 16-bit digitizer with a high-speed USB interface.

For the measured spectra, the wavelength calibration was performed by fitting a high-resolution solar spectrum (Kurucz et al., 1984) to the spectra measured with our instrument. The instrument slit function was assumed to be a Gaussian shape, based on measurements of mercury emission lines around 404.7, 407.8, and 435.8 nm. The wavelength calibration was made daily to take into account temporal changes of wavelength shift and spectral resolution. For the wavelength region analyzed (460–490 nm), the spectral resolution (Full Width at Half Maximum (FWHM)) was about 0.55 nm.

The retrieval algorithm for deriving aerosol information is a 2-step procedure. First, the measured spectra of scattered sunlight at 460–490 nm were analyzed based on the so-called DOAS technique (Platt, 1994) using the nonlinear least-squares spectral fitting method (Levenberg-Marquardt method, Rodgers, 2000) to retrieve the differential

### Performance of MAX-DOAS measurements of aerosols in Japan

H. Irie et al.

Title Page

Abstract

Introduction

Conclusions

References

Tables

Figures

◀

▶

◀

▶

Back

Close

Full Screen / Esc

Printer-friendly Version

Interactive Discussion

slant column density ( $\Delta\text{SCD}$ ) of  $\text{O}_4$ . This spectral fitting was performed with the logarithm of the intensity ( $\ln I$ ). The  $\Delta\text{SCD}$  is defined as the difference between the slant column density along the path of sunlight for an off-axis measurement ( $\text{EL} < 90^\circ$ ) and that for a zenith-sky measurement ( $\text{EL} = 90^\circ$ ). The reference spectrum at time  $t$  was derived by interpolating the two spectra measured at  $\text{EL} = 90^\circ$  within 30 min before and after the off-axis measurement was made at  $t$ . Over 460–490 nm, a wavelength-dependent offset and a slowly-changing structure mainly due to Rayleigh and Mie scattering were taken into account by 2nd- and 3rd-order polynomials, respectively. The gas species considered are  $\text{O}_4$ ,  $\text{NO}_2$ ,  $\text{O}_3$ , and  $\text{H}_2\text{O}$ , for which we adopted absorption cross section data of Greenblatt et al. (1990) (with manual adjustment (A. Richter, personal communication)), Vandaele et al. (1998), Bogumil et al. (2003), and the year 2000 edition of the High-Resolution Transmission (HITRAN) database (Rothman et al., 2003), respectively. In addition, we took into account the Ring effect (Grainger and Ring, 1962) and the undersampling effect using the model of Chance and Spurr (1997) and the method of Chance et al. (2005), respectively. The so-called  $I_0$  effect arising due to different conditions (spectral resolution and light source), under which laboratory experiments of absorption cross sections and atmospheric measurements were made, was considered for all the absorption cross section data, according to the method of Aliwell et al. (2002).

An example of the DOAS spectral fitting results is shown in Fig. 1. In Fig. 1, two spectra of the  $\text{O}_4$  differential optical density ( $\Delta\tau$ ), which correspond to the scaled cross section (red) and the sum of the scaled cross section and the residual (black), respectively, are plotted. The median residual of  $\Delta\tau$  for all the measurements around noon (solar zenith angle ( $\text{SZA}$ ) =  $50^\circ \pm 5^\circ$ ) was as small as  $6 \times 10^{-4}$ . For 6–9 November 2006, the retrieved  $\text{O}_4 \Delta\text{SCD}$  values are shown in Fig. 2. On 6 November cloud bases were persistently detected at altitudes of 3–6 km by lidar over Tsukuba, whereas on 7–9 November the sky was relatively clear. Consistent with the fact that aerosols/clouds lower  $\Delta\text{SCD}$  by shortening the effective path of sunlight reaching the telescope (Wagner et al., 2004),  $\Delta\text{SCD}$  data on 6 November show smaller values and weaker depen-

---

**Performance of  
MAX-DOAS  
measurements of  
aerosols in Japan**H. Irie et al.

---

Title Page

Abstract

Introduction

Conclusions

References

Tables

Figures

◀

▶

◀

▶

Back

Close

Full Screen / Esc

Printer-friendly Version

Interactive Discussion

dences on ELs. These indicate that  $\Delta\text{SCD}$  values were retrieved precisely from our instrumentation and analyses. From 6 to 9 November, a significant temporal variation of aerosols in the lower troposphere is expected to have occurred as  $\Delta\text{SCD}$  values varied over the time period (Fig. 2).

We next use the following methods to convert the  $\text{O}_4\Delta\text{SCD}$  values into  $\tau$  and the vertical profile of  $\sigma$  at  $\lambda=476$  nm. We define the measurement vector ( $\mathbf{y}$ ; representing quantities to be fitted) and the state vector ( $\mathbf{x}$ ; representing quantities to be retrieved) as

$$\mathbf{y} = (\text{O}_4\Delta\text{SCD}(\boldsymbol{\Omega}_1) \quad \dots \quad \text{O}_4\Delta\text{SCD}(\boldsymbol{\Omega}_n))^T \quad \text{and} \quad (1)$$

$$\mathbf{x} = (\tau \quad F_1 \quad F_2 \quad F_3)^T, \quad (2)$$

respectively, where  $n$  is the number of measurements in a 30-min interval and  $\boldsymbol{\Omega}$  the observation geometry vector consisting of three components: the solar zenith angle (SZA), the relative azimuth angle (RAA), and EL. RAA is the azimuth angle between the telescope direction and the Sun.  $F$  values are the parameters determining the shape of a vertical profile and are defined to range between 0 and 1. Thereby, partial  $\tau$  values for 0–1, 1–2, and 2–3 km can be described as  $\tau F_1$ ,  $\tau(1-F_1)F_2$ , and  $\tau(1-F_1)(1-F_2)F_3$ , respectively, and the partial  $\tau$  above 3 km as  $\tau(1-F_1)(1-F_2)(1-F_3)$ .

From the given partial  $\tau$  above 3 km, we determine the profile of  $\sigma$  for a layer from 3 to 100 km assuming a  $\sigma$  value at the top of the layer (100 km) and an exponential profile shape. Similarly, we can determine profiles also for layers of 2–3, 1–2, and 0–1 km, completing the  $\sigma$  vertical profile from the surface to 100 km.

To represent a  $\sigma$  profile with the above method, the prerequisite  $\sigma$  value at 100 km was obtained by extrapolating Stratospheric Aerosol and Gas Experiment III (SAGE III)  $\sigma$  data ( $\lambda=448$  and 521 nm) taken at altitudes of 15–40 km. Although this estimate might be crude, this assumption for high altitudes does not significantly influence the retrieval for the lower troposphere (Frieß et al., 2006). In support of this, a sensitivity test conducted using a tenfold  $\sigma$  value for 100 km showed that its impact on the retrievals of  $\tau$  and  $\sigma$  below 2 km was as small as 3% ( $<0.01$ ).

**Performance of  
MAX-DOAS  
measurements of  
aerosols in Japan**

H. Irie et al.

Title Page

Abstract

Introduction

Conclusions

References

Tables

Figures

◀

▶

◀

▶

Back

Close

Full Screen / Esc

Printer-friendly Version

Interactive Discussion

For different sets of aerosol profiles and observation geometries, we created a lookup table (LUT) of the box-air-mass-factor ( $A_{\text{box}}$ ) vertical profile using our radiative transfer model, the Monte Carlo Atmospheric Radiative Transfer Simulator (MCARaTS) (Iwabuchi, 2006). It has been validated through comparisons with other radiative transfer models (Wagner et al., 2007). The calculations considered the surface altitude at the measurement site and the altitude where the instrument was located (about 30 m above the surface). The present LUT contains more than 300 thousand  $A_{\text{box}}$  profiles in 7 dimensions of  $\tau$ ,  $F_1$ ,  $F_2$ ,  $F_3$ , SZA, RAA, and EL. Each profile has 72 layers for altitudes up to 100 km, with a layer thickness of 100 m for altitudes below 5.1 km. We assumed single values of the single scattering albedo ( $s=0.95$ ), the asymmetry parameter ( $g=0.65$ , under the Henyey-Greenstein approximation), and the surface albedo ( $a=0.10$ ). The sensitivities of all the retrievals (both  $\tau$  and  $\sigma$  values below 2 km) to changing these parameters ( $g$ ,  $s$ , and  $a$ ) by  $\pm 0.05$  were estimated to be as small as 8% ( $\sim 0.01$ ), 2% ( $< 0.01$ ), and 2% ( $< 0.01$ ), respectively.

For off-axis measurement geometries, we also created a LUT for profiles of  $\Delta A_{\text{box}}$ , which was calculated by subtracting the corresponding zenith-sky  $A_{\text{box}}$  value. Instead of  $A_{\text{box}}$ , the  $\Delta A_{\text{box}}$  value was used in the retrieval as it is more directly linked to  $\Delta \text{SCD}$ .

Under the above setup conditions, the  $\tau$  value and the  $\sigma$  profile were retrieved by applying the optimal estimation method (Rodgers, 2000). The a priori values ( $\pm$  error) were set to  $\tau=0.21\pm 1.0$ ,  $F_1=0.70\pm 0.05$ ,  $F_2=0.60\pm 0.05$ , and  $F_3=0.60\pm 0.05$ , based on averages and standard deviations (s.d.) of two months of lidar data mentioned below. This yields a  $\tau$  of 0.21,  $\sigma(0-1 \text{ km})$ , defined as the mean  $\sigma$  for 0–1 km, of  $0.15 \text{ km}^{-1}$ ,  $\sigma(1-2 \text{ km})$  of  $0.04 \text{ km}^{-1}$ , and  $\sigma(2-3 \text{ km})$  of  $0.02 \text{ km}^{-1}$ . The above a priori errors correspond to 20% of the s.d. of  $F$  values from the lidar, but three times for  $\tau$ . This modification was made to stabilize the retrieval and take a wide range of the values. Non-diagonal elements of the a priori covariance matrix were set to zero.

Figure 3 shows the mean averaging kernels for all the MAX-DOAS aerosol retrievals. Except for  $F_3$ , the peaks of the averaging kernels are located at the corresponding variable.  $\tau$  indicates the largest value, followed by  $F_1$  and  $F_2$ , suggesting a higher

## Performance of MAX-DOAS measurements of aerosols in Japan

H. Irie et al.

Title Page

Abstract

Introduction

Conclusions

References

Tables

Figures

◀

▶

◀

▶

Back

Close

Full Screen / Esc

Printer-friendly Version

Interactive Discussion

---

**Performance of  
MAX-DOAS  
measurements of  
aerosols in Japan**

---

H. Irie et al.

[Title Page](#)[Abstract](#)[Introduction](#)[Conclusions](#)[References](#)[Tables](#)[Figures](#)[⏪](#)[⏩](#)[◀](#)[▶](#)[Back](#)[Close](#)[Full Screen / Esc](#)[Printer-friendly Version](#)[Interactive Discussion](#)

sensitivity of MAX-DOAS measurements to lower-altitude aerosols. The resulting degrees of freedom for signal (Rodgers, 2000) ranged from 1.0 to 2.7 for the whole period. The  $O_4\Delta SCD$  values modeled under these conditions (Fig. 4) agreed well with those measured (Fig. 2). For each 30-min interval, the relative residual, (residual of  $O_4\Delta SCD$ )/(mean measured  $O_4\Delta SCD$ ), was calculated. The median of the relative residuals for all the retrievals was 9%.

It should be noted that outputs from the retrieval are available only for retrieved  $\tau$  less than 3, the largest value in the LUTs. This excludes considerably large optical depth cases, most of which should be due to optically thick clouds. Further data screening was made using the relative residual. It would be a good measure for screening the retrievals, which have yielded a  $\sigma$  profile too far from the true profile. This likely happened when the above-mentioned method constructing a profile was too simple to represent the true profile, particularly with a steep vertical gradient of  $\sigma$  due to clouds. From all the retrievals, the threshold for this data screening was determined statistically to be 20%, which corresponded to (the mode) plus (the one-sigma width) in a histogram of the relative residuals on a logarithm basis.

## 2.2 Lidar

The lidar system used here is a compact Mie-scattering system utilizing the second harmonics of a flashlamp-pumped Nd: YAG laser (532 nm) as a light source (Shimizu et al., 2004). One aerosol profile comprising 3000 shots was obtained in 5 min followed by a 10-min rest to extend the laser life. The lidar equation was solved using the inversion method described by Fernald (1984) to derive vertical profiles of aerosol optical properties, such as  $\sigma$ , with a vertical resolution of 30 m. In the method used here, a constant extinction-to-backscattering ratio ( $S$ ) of 50 sr was assumed. According to the estimates by previous studies for Aerosol Robotic Network (AERONET) locations and Tsukuba (Cattrell et al., 2005; Tatarov et al., 2006), the  $S$  ratio can vary by more than 30%, with resulting errors in  $\sigma$  due to the use of a fixed  $S$  value occasionally exceeding 30%. Only  $\sigma$  data, for which no clouds at 0–6 km were judged by the method of

Shimizu et al. (2003), were used below. For reference, vertical profiles of  $\sigma$  at 532 nm measured by the lidar are shown in Fig. 5. We converted the lidar  $\sigma$  values at 532 nm to the values at 476 nm using Ångström exponent data obtained from the sky radiometer measurements described below.

## 5 2.3 Sky radiometer

The sky radiometer measures the direct solar irradiance and the distribution of radiances in the aureole region (Aoki and Fujiyoshi, 2003). In the present study, we analyzed a set of measurements of the direct solar irradiance and the solar aureole radiance distributions within  $160^\circ$  of the center of the Sun. The measurements were made in 30 s to 2 min, depending on SZA, and were repeated every 5 min. The  $\tau$  values at 400, 500, 675, 870, and 1020 nm were derived using the inversion algorithm (SKYRAD.pack, version 4.2) developed by Nakajima et al. (1996). The error in  $\tau$  was generally as small as  $\sim 0.01$  (Kim et al., 2005), comparable to sun photometer measurements implemented in AERONET. Only 30% of the data are used below to minimize the influence by cloud contamination (Aoki and Fujiyoshi, 2003). The Ångström exponent was calculated from the above five  $\tau$  values and was used to derive  $\tau$  at 476 nm.

## 3 Results and discussion

Figure 6a shows the time series of all the MAX-DOAS  $\sigma(0-1 \text{ km})$  values at 476 nm from 1 November to 21 December 2006. The value of  $\sigma(0-1 \text{ km})$  represents the mean value of  $\sigma$  in the layer from 0 to 1 km, as defined earlier. In Fig. 6b, only the coincident pairs of MAX-DOAS (red) and lidar (black) data are plotted. Note that the coincident pairs have been selected using cloud-free lidar data, providing favorable comparison conditions. However, this does not necessarily mean that no clouds occurred at the MAX-DOAS viewing directions. It can readily be seen from Fig. 6b that the MAX-DOAS  $\sigma(0-1 \text{ km})$  values show temporal variations very similar to the lidar data. The

Title Page

Abstract

Introduction

Conclusions

References

Tables

Figures

◀

▶

◀

▶

Back

Close

Full Screen / Esc

Printer-friendly Version

Interactive Discussion

correlations between MAX-DOAS and lidar  $\sigma(0-1 \text{ km})$  values are compact (slope=1.01 and correlation coefficient ( $R^2$ )=0.85), and in most cases the differences are less than 30% (Fig. 7a).

As mentioned above, lidar data have an uncertainty of more than 30%, due to the use of a fixed  $S$  ratio. In addition, MAX-DOAS and lidar measurements were made with different geometries (the combination of zenith-sky and off-axis versus zenith-sky only, respectively) and different integration times for completing a set of measurements (30 versus 5 min, respectively). Because these factors should explain at least part of the differences seen in Fig. 7a, the overall intrinsic uncertainties of MAX-DOAS  $\sigma(0-1 \text{ km})$  are smaller than 30%. Similarly, the uncertainty of the  $\sigma(1-2 \text{ km})$  values was estimated from the comparisons with lidar data (Fig. 7b) to be less than 60%. MAX-DOAS and lidar  $\sigma(2-3 \text{ km})$  values were both about  $0.02 \text{ km}^{-1}$ . However, it was difficult to assess the MAX-DOAS  $\sigma(2-3 \text{ km})$  values, because the values were very close to the a priori value used in the MAX-DOAS retrieval.

It is interesting to note that these comparisons have been made without detailed cloud screening methods for the MAX-DOAS data, and it is very likely that some clouds were occasionally near the FOVs of the MAX-DOAS system, as mentioned above. In the MAX-DOAS/lidar comparisons of  $\sigma$  for the 0–1 km (1–2 km) layer shown in Fig. 7, however, no significant differences exceeding 30% (60%) are generally seen, suggesting that uncertainties due to such cloud influences would be less than 30% (60%).

We next compare  $\tau$  values from MAX-DOAS and the sky radiometer (Fig. 8). Also plotted in Fig. 8b are the mean values of the Moderate Resolution Imaging Spectrometer (MODIS) data (collection 5) obtained within  $0.3^\circ$  latitude and longitude of the measurement site. Two MODIS datasets from different satellites (Terra and Aqua) have been averaged separately but are plotted with the same symbols for simplicity. The MODIS data with a cloud fraction less than 0.2 were used. The original MODIS  $\tau$  values at 470 nm have been converted to those at 476 nm using MODIS Ångström exponent data. Good general agreement between the three datasets can be seen in Fig. 8b.

## Performance of MAX-DOAS measurements of aerosols in Japan

H. Irie et al.

Title Page

Abstract

Introduction

Conclusions

References

Tables

Figures

◀

▶

◀

▶

Back

Close

Full Screen / Esc

Printer-friendly Version

Interactive Discussion

The correlations between MAX-DOAS and sky radiometer data are shown in Fig. 9. For most cases the agreement is within 30% (Fig. 9). However, MAX-DOAS values tend to be smaller than sky radiometer values at sky radiometer  $\tau$  values greater than 0.4 (Fig. 9).

As the sky radiometer tracked the Sun, it was oriented mainly toward the east-southwest sky, whereas the MAX-DOAS measured the sky in a different direction (northwest). In addition, a series of measurements by the sky radiometer was made for an integration time of 30 s to 2 min, which was different from that of MAX-DOAS (30 min). Therefore, the  $\tau$  values in air masses measured by MAX-DOAS and the sky radiometer should have occasionally been different.

These influences of the incomplete matching of the measured air masses might explain the differences between MAX-DOAS and sky radiometer data. It is unlikely, however, that these influences are the dominant factor causing the systematic differences seen at sky radiometer  $\tau$  values greater than 0.4, because they are expected to show random features in the differences.

A simulation of MAX-DOAS aerosol measurements by Frieß et al. (2006) has shown that the sensitivity of the measurements decreases with increasing altitude in the troposphere. This is supported by the averaging kernels for our MAX-DOAS aerosol retrievals (Fig. 3). As discussed above, the profiles of  $\sigma$  from MAX-DOAS agreed well with those from lidar for altitudes below 3 km (Fig. 7). Therefore, the underestimate in MAX-DOAS  $\tau$  values might have occurred, owing to optically thick aerosols above 3 km. This will be confirmed by investigating other sites and seasons, where and when optically thick aerosols occur more often at high altitudes.

Another possible cause is the cloud influence. To quantify the maximum influence of clouds on the MAX-DOAS retrievals, an additional sensitivity test was performed assuming that all extinction occurred by clouds with  $g = 0.86$  and  $s = 1.00$ . The sensitivity test showed that MAX-DOAS  $\tau$  values ( $\sigma$  below 2 km) retrieved assuming typical aerosols ( $g = 0.65$ ,  $s = 0.95$ ) were systematically smaller than those retrieved assuming clouds by about 30% (40%). This result suggests that for more realistic situations con-

## Performance of MAX-DOAS measurements of aerosols in Japan

H. Irie et al.

Title Page

Abstract

Introduction

Conclusions

References

Tables

Figures

◀

▶

◀

▶

Back

Close

Full Screen / Esc

Printer-friendly Version

Interactive Discussion

taining both aerosols and clouds, the  $\tau$  value ( $\sigma$  below 2 km) retrieved assuming typical aerosols includes the 30% (40%)-reduced contribution of the cloud optical depth, possibly explaining part of the systematic differences seen in the comparisons between MAX-DOAS and sky radiometer  $\tau$  data. In addition, this nonnegligible cloud influence qualitatively explains why MAX-DOAS data showed occasional enhancements of  $\tau$  values when no coincidences with sky radiometer measurements under cloud-free conditions occurred (Fig. 8).

Considering the above result suggesting the reduced cloud contribution, the simulation performed by Frieß et al. (2006), and the averaging kernels for our retrieval method, MAX-DOAS measurements would be very insensitive to high-altitude clouds, suggesting that  $\sigma$  profiles in the lower troposphere can be measured even when clouds are present at high altitudes. While MAX-DOAS has these advantages, the development of a proper cloud screening method will improve the performance of aerosol measurements by MAX-DOAS, as well as other remote sensing techniques for aerosol measurements.

## 4 Conclusions

We performed ground-based MAX-DOAS measurements at Tsukuba, Japan, from 1 November to 21 December 2006. To characterize the measurement technique and the retrieval algorithm employed for deriving  $\tau$  and the vertical profile of  $\sigma$  at 476 nm in the lower troposphere, we used comparisons with lidar and sky radiometer measurements. The comparisons between  $\sigma(0-1\text{ km})$  values from MAX-DOAS and the lidar showed good agreement, within 30% for most cases, although the cases compared probably included partly cloudy conditions. Considering that errors in lidar  $\sigma$  data could occasionally exceed 30%, it is likely that the comparisons yielded an upper limit to the overall uncertainty of MAX-DOAS  $\sigma(0-1\text{ km})$  data. Similarly, the overall uncertainty of MAX-DOAS  $\sigma(1-2\text{ km})$  was estimated to be less than 60%. The MAX-DOAS  $\tau$  values generally agreed with sky radiometer data to within 30%. MAX-DOAS thus provides a

### Performance of MAX-DOAS measurements of aerosols in Japan

H. Irie et al.

Title Page

Abstract

Introduction

Conclusions

References

Tables

Figures

⏪

⏩

◀

▶

Back

Close

Full Screen / Esc

Printer-friendly Version

Interactive Discussion

new dataset of aerosols in the troposphere. Moreover, the derived aerosol properties can be used as reliable input parameters for the vertical profile retrieval of trace gases detected by MAX-DOAS. In some cases, however, the MAX-DOAS  $\tau$  values tended to be smaller than sky radiometer data. This underestimation likely occurred when optically thick aerosols were present at high altitudes and/or clouds occurred in the lower troposphere. It was suggested that  $\sigma$  profiles can be measured by MAX-DOAS even when clouds are present at high altitudes. However, the development of a proper cloud screening method is highly desirable for more accurate aerosol measurements by MAX-DOAS.

*Acknowledgements.* The authors thank T. Wagner for providing absorption cross section data. We are grateful to K. Chance for providing the Ring calculation model. MODIS data were obtained from the NASA LAADS web site. This work was supported by Global Environment Research fund (B-051) and Japan EOS Promotion Program (JEPP).

## References

- Aoki, K. and Fujiyoshi, Y.: Sky radiometer measurements of aerosol optical properties over Sapporo, Japan, *J. Meteorol. Soc. Jpn.*, 81(3), 493–513, 2003.
- Aliwell, S. R., van Roozendael, M., Johnston, P. V., Richter, A., Wagner, T., Arlander, D. W., Burrows, J. P., Fish, D. J., Jones, R. L., Tørnkvist, K. K., Lambert, J.-C., Pfeilsticker, K., and Pundt, I.: Analysis for BrO in zenith-sky spectra: An intercomparison exercise for analysis improvement, *J. Geophys. Res.*, 107(D14), 4199, doi:10.1029/2001JD000329, 2002.
- Bogumil, K., Orphal, J., Homann, T., Voigt, S., Spietz, P., Fleischmann, O. C., Vogel, A., Hartmann, M., Bovensmann, H., Frerik, J., and Burrows, J. P.: Measurements of molecular absorption spectra with the SCIAMACHY pre-flight model: Instrument characterization and reference data for atmospheric remote-sensing in the 230–2380 nm region, *J. Photochem. Photobiol. A.*, 157, 167–184, 2003.
- Catrrall, C., Reagan, J., Thome, K., and Dubovik, O.: Variability of aerosol and spectral lidar and backscatter and extinction ratios of key aerosol types derived from selected Aerosol Robotic Network locations, *J. Geophys. Res.*, 110, D10S11, doi:10.1029/2004JD005124, 2005.

## Performance of MAX-DOAS measurements of aerosols in Japan

H. Irie et al.

Title Page

Abstract

Introduction

Conclusions

References

Tables

Figures

⏪

⏩

◀

▶

Back

Close

Full Screen / Esc

Printer-friendly Version

Interactive Discussion

---

**Performance of  
MAX-DOAS  
measurements of  
aerosols in Japan**H. Irie et al.

---

Title Page

Abstract

Introduction

Conclusions

References

Tables

Figures

⏪

⏩

◀

▶

Back

Close

Full Screen / Esc

Printer-friendly Version

Interactive Discussion

Chance, K. and Spurr, R. J. D.: Ring effect studies: Rayleigh scattering, including molecular parameters for rotational Raman scattering, and the Fraunhofer spectrum, *Appl. Opt.*, 36, 5224–5230, 1997.

Chance, K., Kurosu, T. P., and Sioris, C. E.: Undersampling correction for array detector-based satellite spectrometers, *Appl. Opt.*, 44(7), 1296–1304, 2005.

Fernald, F. G.: Analysis of atmospheric lidar observations: some comments, *Appl. Opt.*, 23(5), 652–653, 1984.

Frieß, U., Monks, P. S., Remedios, J. J., Rozanov, A., Sinreich, R., Wagner, T., and Platt, U.: MAX-DOAS O<sub>4</sub> measurements: A new technique to derive information on atmospheric aerosols: 2. Modeling studies, *J. Geophys. Res.*, 111, D14203, doi:10.1029/2005JD006618, 2006.

Grainger, J. F. and Ring, J.: Anomalous Fraunhofer line profiles, *Nature* 193, 762, 1962.

Greenblatt, G. D., Orlando, J. J., Burkholder, J. B., and Ravishankara, A. R.: Absorption measurements of oxygen between 330 and 1140 nm, *J. Geophys. Res.*, 95, 11, 18 577–18 582, 1990.

Heckel, A., Richter, A., Tarsu, T., Wittrock, F., Hak, C., Pundt, I., Junkermann, W., and Burrows, J. P.: MAX-DOAS measurements of formaldehyde in the Po-Valley, *Atmos. Chem. Phys.*, 5, 909–918, 2005,

<http://www.atmos-chem-phys.net/5/909/2005/>.

Hendrick, F., van Roozendaal, M., Kylling, A., Petritoli, A., Rozanov, A., Sanghavi, S., Schofield, R., von Friedeburg, C., Wagner, T., Wittrock, F., Fonteyn, D., and De Mazière, M.: Intercomparison exercise between different radiative transfer models used for the interpretation of ground-based zenith-sky and multi-axis DOAS observations, *Atmos. Chem. Phys.*, 6, 93–108, 2006,

<http://www.atmos-chem-phys.net/6/93/2006/>.

Hönninger, G., von Friedeburg, C., and Platt, U.: Multi axis differential optical absorption spectroscopy (MAX-DOAS), *Atmos. Chem. Phys.*, 4, 231–254, 2004,

<http://www.atmos-chem-phys.net/4/231/2004/>.

Iwabuchi, H.: Efficient Monte Carlo methods for radiative transfer modeling, *J. Atmos. Sci.*, 63(9), 2324–2339, 2006.

Kaufman, Y. J., Tanré, D., and Boucher, O.: A satellite view of aerosols in the climate system, *Rev. Nature*, 419, 215–223, 2002.

Kim, D.-H., Sohn, B. J., Nakajima, T., and Takamura, T.: Aerosol radiative forcing over east

**Performance of  
MAX-DOAS  
measurements of  
aerosols in Japan**

H. Irie et al.

Title Page

Abstract

Introduction

Conclusions

References

Tables

Figures

◀

▶

◀

▶

Back

Close

Full Screen / Esc

Printer-friendly Version

Interactive Discussion

Asia determined from ground-based solar radiation measurements, *J. Geophys. Res.*, 110, D10S22, doi:10.1029/2004JD004678, 2005.

Kurucz, R. L., Furenid, I., Brault, J., and Testerman, L.: Solar flux atlas from 296 to 1300 nm, *Natl. Sol. Obs., Sunspot, New Mexico*, 240pp., 1984.

5 Leigh, R. J., Corlett, G. K., Frieß, U., and Monks, P. S.: Concurrent multiaxis differential optical absorption spectroscopy system for the measurement of tropospheric nitrogen dioxide, *Appl. Opt.*, 45, 28, 7504–7518, 2006.

Nakajima, T., Tonna, G., Rao, R., Boi, P., Kaufman, Y., and Holben, B.: Use of sky brightness measurements from ground for remote sensing of particulate polydispersions, *Appl. Opt.*, 35(15), 2672–2686, 1996.

10 Platt, U.: Differential optical absorption spectroscopy (DOAS), *Air Monitoring by Spectroscopic Techniques*, edited by: Sgrist, M. W., John Wiley & Sons, Inc., New York, 127, 27–84, 1994.

Rodgers, C. D.: Inverse methods for atmospheric sounding: Theory and practice, *Ser. Atmos. Oceanic Planet. Phys.*, 2, edited by: Taylor, F. W., World Sci., Hackensack, N. J., 2000.

15 Rothman, L. S., Barbe, A., Benner, D. C., Brown, L. R., Camy-Peyret, C., Carleer, M. R., Chance, K., Clerbaux, C., Dana, V., Devi, V. M., Fayt, A., Flaud, J.-M., Gamache, R. R., Goldman, A., Jacquemart, D., Jucks, K. W., Lafferty, W. J., Mandin, J.-Y., Massie, S. T., Nemtchinov, V., Newnham, D. A., Perrin, A., Rinsland, C. P., Schroeder, J., Smith, K. M., Smith, M. A. H., Tang, K., Toth, R. A., Vander Auwera, J., Varanasi, P., and Yoshino, K.: The HITRAN molecular spectroscopic database: edition of 2000 including updates through 2001, *J. Quant. Spectrosc. Radiat. Transfer*, 82, 5–44, 2003.

20 Shimizu, A., Sugimoto, N., Matsui, I., Arai, K., Uno, I., Murayama, T., Kagawa, N., Aoki, K., Uchiyama, A., and Yamazaki, A.: Continuous observations of Asian dust and other aerosols by polarization lidars in China and Japan during ACE-Asia, *J. Geophys. Res.*, 109, D19S17, doi:10.1029/2002JD003253, 2004.

Sinreich, R., Volkamer, R., Filsinger, F., Frieß, U., Kern, C., Platt, U., Sebastian, O., and Wagner, T.: MAX-DOAS detection of glyoxal during ICARTT 2004, *Atmos. Chem. Phys.*, 7, 1293–1303, 2007,

<http://www.atmos-chem-phys.net/7/1293/2007/>.

30 Tatarov, B., Sugimoto, N., Matsui, I., and Shimizu, A.: Two-year-observations of optical properties of the tropospheric aerosol and clouds by a high-spectral-resolution lidar over Tsukuba, Japan, *Reviewed and Revised Papers Presented at the 23rd International Laser Radar Conference*, 23ILRC, ISBN 4-9902916-0-3, 451–454, 2006.

Vandaele, A. C., Hermans, C., Simon, P. C., Carleer, M., Colin, R., Fally, S., Mérienne, M. F., Jenouvrier, A., and Coquart, B.: Measurements of the NO<sub>2</sub> absorption cross-section from 42 000 cm<sup>-1</sup> to 10 000 cm<sup>-1</sup> (238–1000 nm) at 220 K and 294 K, *J. Quant. Spectrosc. Radiat. Transfer*, 59, 171–184, 1998.

5 Wagner, T., Dix, B., von Friedeburg, C., Frieß, U., Sanghavi, S., Sinreich, R., and Platt, U.: MAX-DOAS O<sub>4</sub> measurements: A new technique to derive information on atmospheric aerosols – Principles and information content, *J. Geophys. Res.*, 109, D22205, doi:10.1029/2004JD004904, 2004.

10 Wagner, T., Burrows, J. P., Deutschmann, T., Dix, B., von Friedeburg, C., Frieß, U., Hendrick, F., Heue, K.-P., Irie, H., Iwabuchi, H., Kanaya, Y., Keller, J., McLinden, C. A., Oetjen, H., Palazzi, E., Petritoli, A., Platt, U., Postlyakov, O., Pukite, J., Richter, A., van Roozendaal, M., Rozanov, A., Rozanov, V., Sinreich, R., Sanghavi, S., and Wittrock, F.: Comparison of box-air-mass-factors and radiances for multiple-axis differential optical absorption spectroscopy (MAX-DOAS) geometries calculated from different UV/visible radiative transfer models, *Atmos. Chem. Phys.*, 7, 1809–1833, 2007,  
15 <http://www.atmos-chem-phys.net/7/1809/2007/>.

Wittrock, F., Oetjen, H., Richter, A., Fietkau, S., Medeke, T., Rozanov, A., and Burrows, J. P.: MAX-DOAS measurements of atmospheric trace gases in Ny-Ålesund – Radiative transfer studies and their application, *Atmos. Chem. Phys.*, 4, 955–966, 2004,  
20 <http://www.atmos-chem-phys.net/4/955/2004/>.

---

**Performance of  
MAX-DOAS  
measurements of  
aerosols in Japan**

H. Irie et al.

---

Title Page

Abstract

Introduction

Conclusions

References

Tables

Figures

⏪

⏩

◀

▶

Back

Close

Full Screen / Esc

Printer-friendly Version

Interactive Discussion

**Performance of  
MAX-DOAS  
measurements of  
aerosols in Japan**

H. Irie et al.

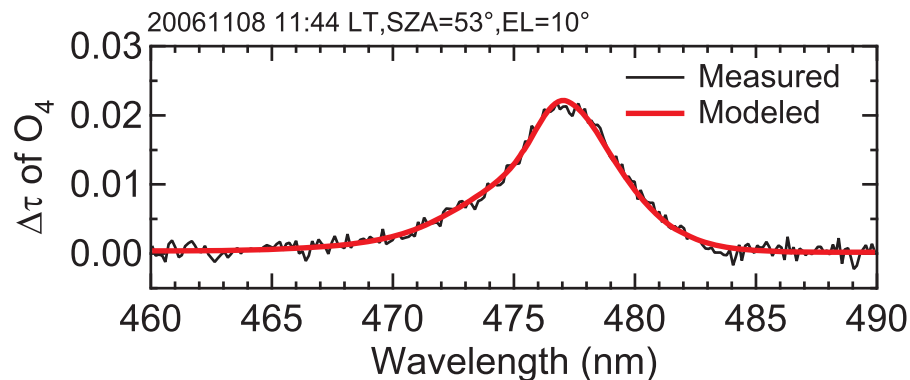


**Fig. 1.** Example of nonlinear least-squares spectral fitting results for  $O_4$ . This is for SZA=53° and EL=10° on 8 November 2006. The red line shows the cross section scaled to the measured spectrum (black) by the DOAS technique. The spectra are plotted as a differential optical density ( $\Delta\tau$ ) from the reference spectrum (EL=90°).

[Title Page](#)[Abstract](#)[Introduction](#)[Conclusions](#)[References](#)[Tables](#)[Figures](#)[◀](#)[▶](#)[◀](#)[▶](#)[Back](#)[Close](#)[Full Screen / Esc](#)[Printer-friendly Version](#)[Interactive Discussion](#)

**Performance of  
MAX-DOAS  
measurements of  
aerosols in Japan**

H. Irie et al.

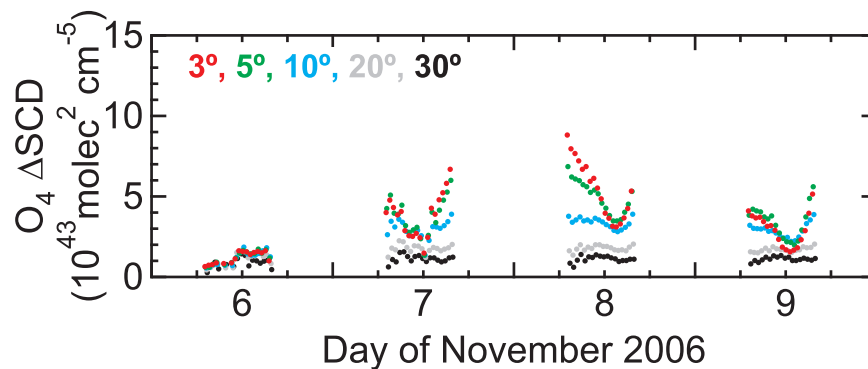


**Fig. 2.** Time series of  $O_4 \Delta SCD$  values at EL=3° (red), 5° (green), 10° (blue), 20° (gray), and 30° (black) on 6–9 November 2006.

[Title Page](#)[Abstract](#)[Introduction](#)[Conclusions](#)[References](#)[Tables](#)[Figures](#)[◀](#)[▶](#)[◀](#)[▶](#)[Back](#)[Close](#)[Full Screen / Esc](#)[Printer-friendly Version](#)[Interactive Discussion](#)

**Performance of  
MAX-DOAS  
measurements of  
aerosols in Japan**

H. Irie et al.

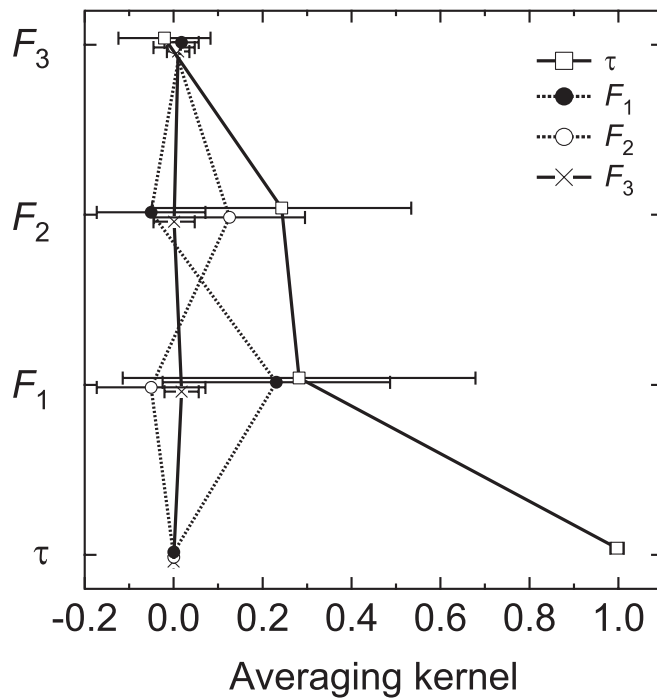


**Fig. 3.** Mean averaging kernels for all the MAX-DOAS aerosol retrievals. Error bars represent  $1\sigma$  standard deviations.

[Title Page](#)[Abstract](#)[Introduction](#)[Conclusions](#)[References](#)[Tables](#)[Figures](#)[◀](#)[▶](#)[◀](#)[▶](#)[Back](#)[Close](#)[Full Screen / Esc](#)[Printer-friendly Version](#)[Interactive Discussion](#)

**Performance of  
MAX-DOAS  
measurements of  
aerosols in Japan**

H. Irie et al.

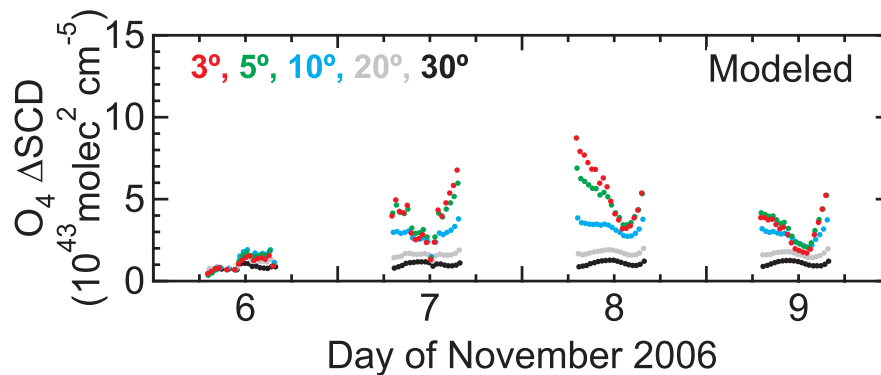


**Fig. 4.** Same as Fig. 2, but for the modeled  $O_4 \Delta SCD$  values.

[Title Page](#)[Abstract](#)[Introduction](#)[Conclusions](#)[References](#)[Tables](#)[Figures](#)[◀](#)[▶](#)[◀](#)[▶](#)[Back](#)[Close](#)[Full Screen / Esc](#)[Printer-friendly Version](#)[Interactive Discussion](#)

**Performance of  
MAX-DOAS  
measurements of  
aerosols in Japan**

H. Irie et al.

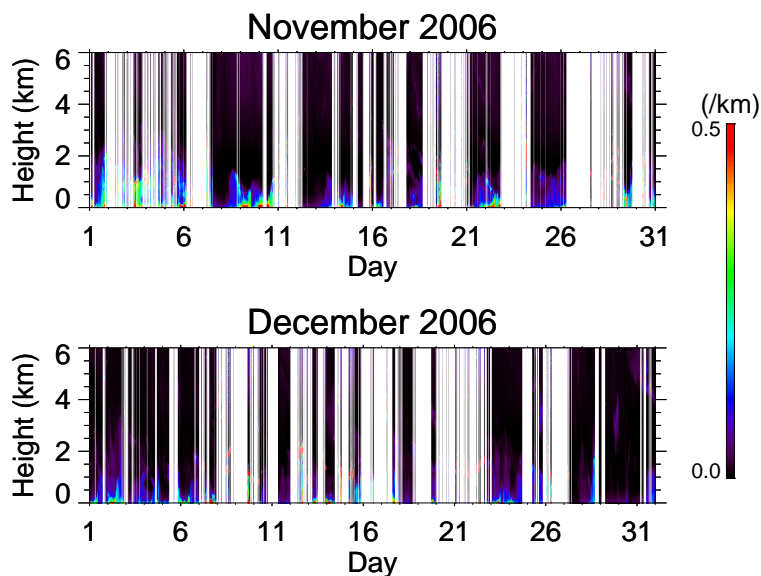


**Fig. 5.** Vertical profiles of the lidar aerosol extinction coefficient ( $\sigma$ ) data at 532 nm for (top) November and (bottom) December 2006.

[Title Page](#)[Abstract](#)[Introduction](#)[Conclusions](#)[References](#)[Tables](#)[Figures](#)[◀](#)[▶](#)[◀](#)[▶](#)[Back](#)[Close](#)[Full Screen / Esc](#)[Printer-friendly Version](#)[Interactive Discussion](#)

**Performance of  
MAX-DOAS  
measurements of  
aerosols in Japan**

H. Irie et al.

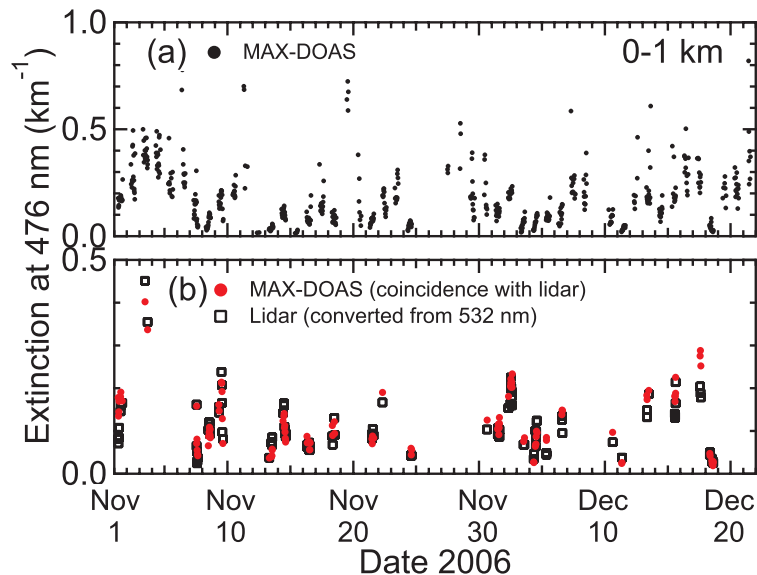


**Fig. 6.** (a) Time series of all the MAX-DOAS aerosol extinction coefficient ( $\sigma$ ) data at 476 nm for the layer from 0 to 1 km. (b) Only coincident MAX-DOAS (red) and lidar (black) data are shown. Original lidar data have been converted to the values at 476 nm using the Ångström exponent derived from sky radiometer data.

[Title Page](#)[Abstract](#)[Introduction](#)[Conclusions](#)[References](#)[Tables](#)[Figures](#)[◀](#)[▶](#)[◀](#)[▶](#)[Back](#)[Close](#)[Full Screen / Esc](#)[Printer-friendly Version](#)[Interactive Discussion](#)

**Performance of  
MAX-DOAS  
measurements of  
aerosols in Japan**

H. Irie et al.

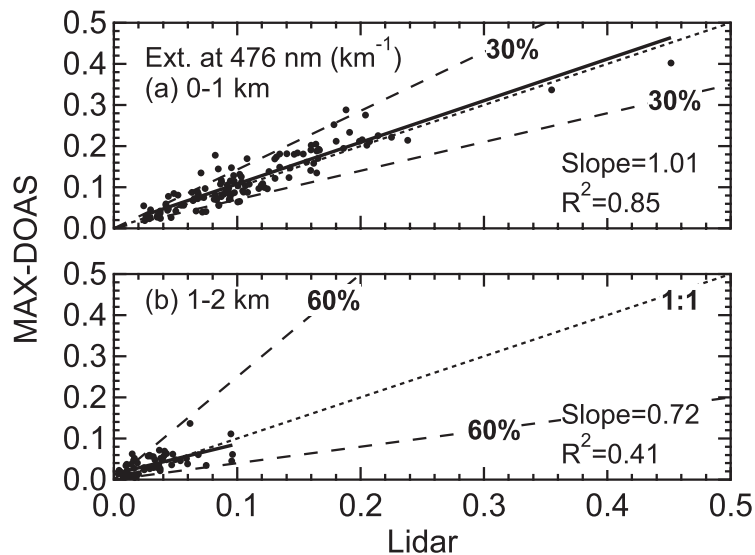


**Fig. 7.** Correlations between  $\sigma$  values from MAX-DOAS and lidar for layers of **(a)** 0–1 and **(b)** 1–2 km. The 1:1 relationship and the 30% range are represented by the dotted line and dashed lines, respectively.

[Title Page](#)[Abstract](#)[Introduction](#)[Conclusions](#)[References](#)[Tables](#)[Figures](#)[◀](#)[▶](#)[◀](#)[▶](#)[Back](#)[Close](#)[Full Screen / Esc](#)[Printer-friendly Version](#)[Interactive Discussion](#)

**Performance of  
MAX-DOAS  
measurements of  
aerosols in Japan**

H. Irie et al.

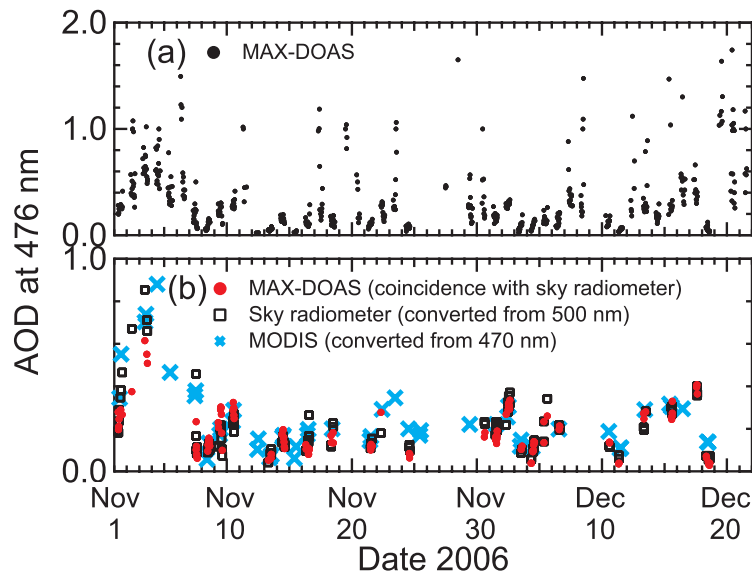


**Fig. 8.** (a) Time series of all the MAX-DOAS  $\tau$  (AOD) data at 476 nm. (b) Only coincident MAX-DOAS (red) and sky radiometer (black) data are shown. For reference, MODIS  $\tau$  data (sky blue) are also plotted. The original sky radiometer and MODIS data have been converted to the values at 476 nm using the Ångström exponent.

[Title Page](#)[Abstract](#)[Introduction](#)[Conclusions](#)[References](#)[Tables](#)[Figures](#)[◀](#)[▶](#)[◀](#)[▶](#)[Back](#)[Close](#)[Full Screen / Esc](#)[Printer-friendly Version](#)[Interactive Discussion](#)

**Performance of  
MAX-DOAS  
measurements of  
aerosols in Japan**

H. Irie et al.

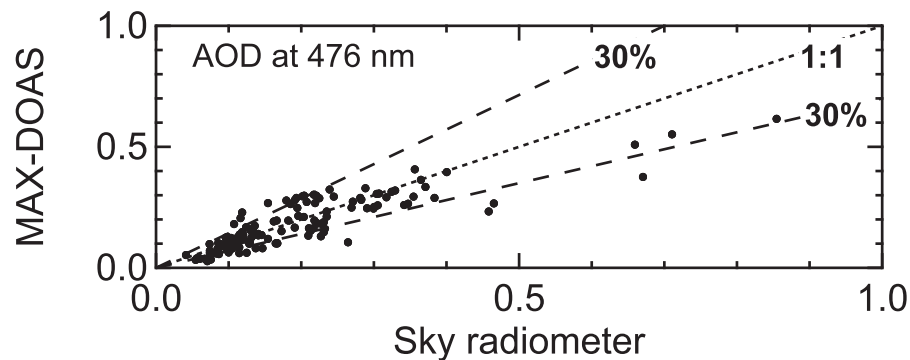


**Fig. 9.** Same as Fig. 7, but for the correlations between  $\tau$  (AOD) values at 476 nm from MAX-DOAS and sky radiometer data.

[Title Page](#)[Abstract](#)[Introduction](#)[Conclusions](#)[References](#)[Tables](#)[Figures](#)[◀](#)[▶](#)[◀](#)[▶](#)[Back](#)[Close](#)[Full Screen / Esc](#)[Printer-friendly Version](#)[Interactive Discussion](#)